Isogeometric approach to Strain Gradient Plasticity theories

Kocherla Amar Teja

A Thesis Submitted to

Indian Institute of Technology Hyderabad

In Partial Fulfillment of the Requirements for

The Degree of Master of Technology

Department of Civil Engineering

July 2015

Approval Sheet

This Thesis entitled Isogeometric approach to Strain Gradient Plasticity theories by Kocherla Amar Teja is approved for the degree of Master of Technology from IIT Hyderabad

(Prof. Saswata Battacharya) Examiner
Dept. of Mat Science and Eng
IITH

(Prof. Anil Agarwal) Examiner
Dept. of Civil Eng
IITH

(Dr. Amirtham Rajagopal) Adviser 10/7/15
Dept. of Civil Eng
IITH

Declaration

I declare that this written submission represents my ideas in my own words, and where others' ideas or words have been included, I have adequately cited and referenced the original sources. I also declare that I have adhered to all principles of academic honesty and integrity and have not misrepresented or fabricated or falsified any idea/data/fact/source in my submission. I understand that any violation of the above will be a cause for disciplinary action by the Institute and can also evoke penal action from the sources that have thus not been properly cited, or from whom proper permission has not been taken when needed.

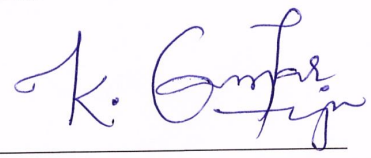

KOCHERLA AMARTEJA

CE13M1002

Acknowledgements

I am grateful to my advisor, Dr. Amirtham Rajagopal, for his advice and encouragement during the course of my graduate studies at IIT Hyderabad. I also thank Prof. K. V. L. Subramaniam, Prof. Saswata Battacharya and Prof. Anil Agarwal for serving on my thesis committee. I have greatly benefited from the friendship and association with many individuals during the course of my study at IIT Hyderabad. Finally, I would like to express my whole-hearted gratitude to my parents for the values they instilled in me, and for their love and support in my academic endeavors.

Abstract

Structural materials display a strong size dependence when deformed non uniformly into the inelastic range:smaller is stronger. This effect has important implications for an increasing number of applications in structural failure. The mechanical behavior of these applications cannot be characterized by classical continuum theories because they incorporate no material length scales and consequently predict no size effects. On the other hand , it is still not possible to perform quantum and atomistic simulations in order to be able to design the size dependent structures of modern technology Nonlocal rate dependent and gradient dependent theories of plasticity and damage are developed in this work for this purpose. we adopt a multi scale hierarchical thermodynamic consistent framework to construct the material constitutive relations for the scale dependent plasticity behavior. Material length scales are implicitly or explicitly introduced into the governing equations through material rate dependency and coefficients of spatial higher order gradients of one or more material state variables, respectively.

The finite element simulations of material instability problems converge to meaningful results upon further refinement of the finite element mesh, since the width of the fracture process zone is determinded by the intristic material scales; While the classical continuum theories fail to address this problem. It is also shown that the proposed theory is successful for the interproetation of indentation size effects in micro hardness. Future studies should be directed toward incorporation of the size effects into design procedures and code recommendations of modern engineering structures

Contents

Chapter 1

Introduction

The goal of this thesis is a physically motivated and thermodynamically consistent formulation of higher gradient inelastic material behavior. Thereby, the influence of the material micro-structure is incorporated. Two major inelastic effects will be addressed in this thesis. The first one is elasto-plastic processes and the other is damage mechanisms, which will be modeled within a continuum mechanics framework. In particular, focus will be on ductile materials. For example, steel that plays an important role in engineering, possess desirable characteristics at various length scales. The structural materials (like steel) display a strong size-dependence when deformed non-uniformly into the inelastic range. This inelastic behavior can be treated with in the framework of small deformations. The mechanical behavior of these applications cannot be characterized by classical (local) continuum theories because they incorporate no material length scales and consequently predict no size effects. It is therefore necessary to develop a scale-dependent continuum theory in order to design the size-dependent structures of modern technology.

And the Observation of the mechanical behavior and failure of various materials reveals the existence of localization phenomena. Strain localization is a notion describing a deformation mode, in which whole deformation of a material specimen occurs in one or more narrow bands, while the rest of the specimen usually exhibits unloading and then finally the softening effect prevails and leads to material instabilities. And in this softening regime, due to large deformation gradients, the characteristic deformation scale and micro-structure size become comparable. These large deformation gradients causes relative motion of micro-structures which contributes to deformation of body. Moreover, the micro-structures interact over distances comparable to the length scale in the deformation pattern, which means that state of the material at a point depends on deformation history of a certain neighborhood of this point. So, to assess the safety of a system in softening response it is necessary to analyze its ductility. Therefore, there exists a demand for reliable computational methods capable of reproducing post peak behavior in addition to ultimate load carrying capacity. One of the most effective tools for the numerical computation of such phenomena is offered by the Finite Element Method. But the deficiencies of classical local continuum models become particularly obvious in the post-critical regime in terms of pathological dependency from the chosen discretization. This can be mathematically translated into a loss of ellipticity of the governing equations. It renders physically meaningless results. For example, shear bands of zero width are computed for ductile materials that are discretized in the limit with an infinite fine mesh. Over the past decade,

much research has therefore been dedicated to modifications of standard local continuum descriptions. These so-called regularizations try to resolve micro-structural interactions by introducing an internal length scale. One of the most promising approaches is based on the incorporation of higher gradients.

When material exhibits inelastic behavior, then one can identify dislocations and dislocation motion. These dislocations can encounter obstacles and get pinned. The number of dislocations increases dramatically during this inelastic deformation. The average distance between dislocations decreases and dislocations start blocking the motion of each other. Plastic deformation increases the dislocation density and changes grain size distributions resulting in material hardening. So, dislocation densities and incompatibilities are identified to influence the hardening behavior, in particular, geometrically necessary dislocations, which can be related to the gradient of the classical hardening variable and have to be taken into account. This leads to complex coupled non-linear boundary value problems that can mainly be solved in an approximated manner with the help of numerical methods. It thus seems suitable to generally incorporate the gradient of an internal variable into the Helmholtz free energy in order to set up a phenomenological continuum theory of inelastic material behavior. Remarkably, the micro-structural influence is thereby incorporated based on physical arguments. This finally renders the algorithmic solution of a coupled problem culminating in a two-field finite element formulation. In gradient plasticity, spatial derivatives of the inelastic state variables enter the constitutive description of solid apart from the inelastic state variables themselves.

1.1 Concepts of the formulation of inelastic materials with microstructure

In standard local continuum formulations, micro-structural interactions are neglected. That means no reference to any characteristic length accounting for the structural size of the material is incorporated. There are nevertheless several evidences for micro-structural interactions within plastic deformation phenomena. Furthermore, recent micro-scale experiments support the size effect especially in metals. The underlying physical interpretation is related to the development of geometrically necessary dislocations that cause enhanced hardening. Thereby, the continuum dislocation theory provides a strong tool relating the geometrically necessary dislocations to the higher gradients of the state variables.

Apart from the physical considerations that micro-structural interactions have to be taken into account to fully describe inelastic material behavior, there are shortcomings with respect to the computational treatment of classical local materials that are simple in the sense of [1] and exhibit softening. They fail to provide mesh objective results after the onset of localization, that translates mathematically into a loss of ellipticity of the governing equations as outlined in [2]. This renders physically meaningless results which are displayed in a vanishing localized zone and zero amount of dissipated energy driving the failure process.

Among the most effective remedies against the non-physical behavior displayed by a softening standard continuum and its numerical computation, nonstandard continuum theories have been proposed. On the one hand, one may thereby distinguish theories, which introduce extra internal degrees of freedom that result in couple stresses. On the other hand, the introduction of internal

variables and their nonlocal counterparts (eg., gradients), reflects the microstructural response.

1.2 Internal Variables

On the one hand, the incorporation of micro-structure in terms of internal variables and their spatial gradients, in particular, higher order displacement gradients, dates back to [3], [4], [5]. Further developments were analyzed by [6] and [7]. Beforehand, [8] coined the notion of localization limiters. A variational framework to gradient plasticity was proposed by [9] and a corresponding gradient theory of phenomenological plasticity was developed by [10]. The gradient effect is frequently incorporated by a Laplacian of the internal variable into the yield condition, see [11]. On the other hand, microstructural interactions are introduced in terms of internal variables and their nonlocal counterparts by Eringen. The non-locality is obtained by weighted averaging over a spatial neighborhood of a local quantity. The universality of thermodynamics with internal variables seems intriguing because of its conceptual beauty since it does not require additional balance laws. The Fundamentals of Rational Thermodynamics, in particular the consistency with the second law of thermodynamics, are invoked.

Chapter 2

Isogeometric Analysis

2.1 Underlying concepts of Isogeometric Analysis

The predominant technology that is used by CAD to represent complex geometries is the Non-Uniform Rational B-spline (NURBS). This allows certain geometries to be represented exactly that can only be approximated by polynomial functions, such as conic and circular sections. There is a vast array of literature focused on Non-Uniform Rational B-splines (NURBS) and as a result of several decades of research, many ecient computer algorithms exist for their fast evaluation and renement. The key observation that was made by Hughes was that NURBS can not only be used to describe the geometry of a problem, but can also be used to construct nite approximations for analysis and coined the phrase Isogeometric Analysis (IGA).

2.2 B-Splines

In this section a brief discussion on B-splines is given since the same technology is utilized for more advanced geometrical functions.

2.2.1 Knot vectors

A knot vector is a sequence in ascending order of parameter values, written as $E = \xi 1, \xi 2, ...\xi_{n+p+1}$, where, ξ_i is the i^{th} knot, n is the number of basis functions and p is the polynomial order. The knot vector divides the parametric space into intervals usually referred as knot spans. Consecutive knots can have the same value i.e., more than one knot can be located at the same coordinate in the parametric space. A number of coinciding knots is referred to as a knot with a certain multiplicity. A knot vector is said to b a open if its first and last knots have multiplicity equal to the polynomial order plus one (p+1). An important property of open knot vectors is that the resulting basis funcions are interpolatory at the ends of the paramtric space. A uniform knot vector is associated to evenly distributed knots. Otherwise, it is said to be a non uniform knot vector.

2.2.2 B-spline Basis functions

Given a knot vector, the B-spline basis functions are defined recursively starting with the zeroth order basis function ($p = 0$) as

$$N_{i,0}(\xi) = \begin{cases} 1, & \text{if } \xi_i \leq \xi < \xi_{i+1} \\ 0, & \text{otherwise} \end{cases} \tag{2.1}$$

First and higher order basis can be calculated as

$$N_{i,p}(\xi) = \frac{\xi - \xi_i}{\xi_{i+p} - \xi_i} N_{i,p-1}(\xi) + \frac{\xi_{i+p+1} - \xi}{\xi_{i+p+1} - \xi_{i+1}} N_{i+1,p-1}(\xi) \tag{2.2}$$

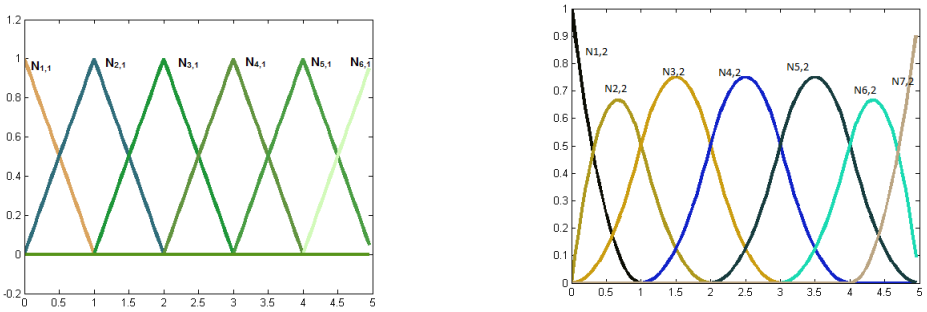

(a) First order basis functions

(b) Second order basis functions

Figure 2.1: B-spline basis functions in one and two dimensions

Derivatives of B-spline basis functions can be written as

$$\frac{d}{d\xi} N_{i,p}(\xi) = \frac{p}{\xi_{i+p+1} - \xi_{i+1}} N_{i+1,p-1}(\xi) \tag{2.3}$$

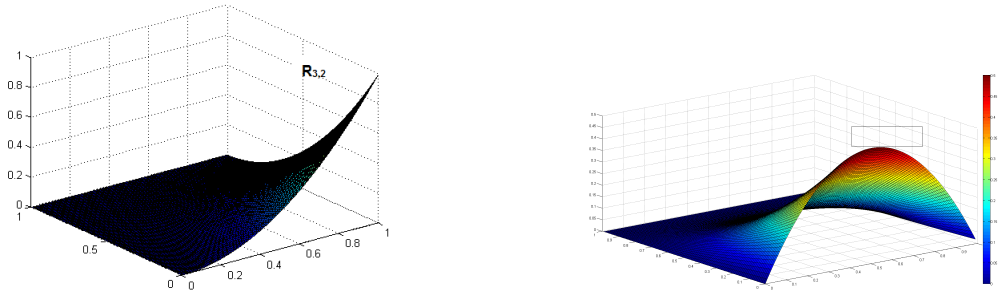

(a) First order basis functions

(b) Second order basis functions

Figure 2.2: B-spline basis functions in one and two dimensions

Note that for $p = 0$ and $p = 1$, the basis functions are the same as for standard piecewise constant and linear finite element functions, respectively. However, for $p \geq 2$, they are different. Quadratic B-spline basis functions (and NURBS basis functions, as will be shown later) are identical but shifted.

This is in contrast with quadratic finite element functions which are different for internal and end nodes. Note that the basis functions are interpolatory at the ends of the interval, the location of a repeated knot, where only C^0 continuity is attained. Elsewhere, the functions are C^1 continuous. In general, basis functions of order p have $(p-1)$ continuous derivatives. If a knot is repeated k times, then the number of continuous derivatives decreases by k. When the multiplicity of a knot is exactly p, the basis function is interpolatory.

2.2.3 B-spline Properties

- B-spline basis functions constitute a partion of unity.

$$\sum_{i=1}^{n} \boldsymbol{N}_{i,p}(\xi) = 1 \tag{2.4}$$

- Each basis function is nonnegative over the entire domain.

$$\boldsymbol{N}_{i,p}(\xi) \geq 0 \tag{2.5}$$

- B-spline basis functions are linearly independent.

$$\sum_{i=1}^{n} \alpha_i \boldsymbol{N}_i(\xi) = 0 \tag{2.6}$$

- The support of a B-spline function of order p is $(p+1)$ knot spans, i.e., $\boldsymbol{N}_{i,p}$ is non zero over $[\xi_i, \xi_{i+p+1}]$.

- B-spline basis are generally only approximants and not interpolants. that is they do not satisfy the Kronecker delta property.

$$\boldsymbol{N}_{i,p}(\xi_j) \neq \delta_{ij} \tag{2.7}$$

- Only in the case of $m_i = p$, then $\boldsymbol{N}_{i,p}(\xi_i) = 1$

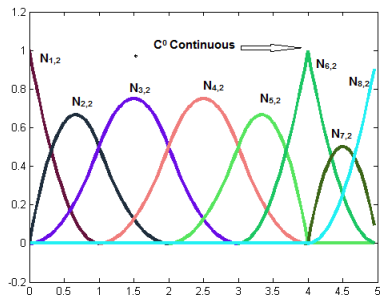

(a) Repeated knot

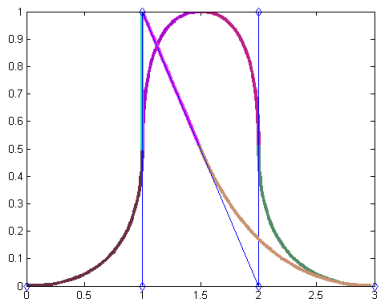

(b) Repeated control point

2.2.4 B-spline curve

B-spline curves are constructed by taking a linear combination of B-spline basis functions. The coefficients of the basis functions are referred to as control points. These are somewhat analogous to nodal coordinates in finite element analysis. Piecewise linear interpolation of the control points gives the so-called control polygon. In general, control points are not interpolated by B-spline curves. Given n basis functions and their corresponding control points, a piecewise polynomial B-spline curve can be written as

$$\mathcal{C}(\xi) = \sum_{i=1}^{n} N_{i,p}(\xi)\mathcal{B}_i \tag{2.8}$$

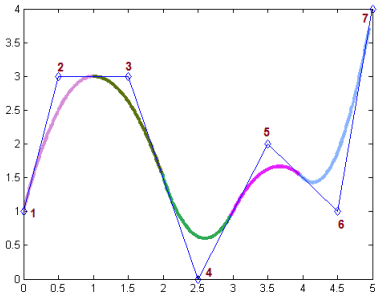

(c) B-spline curve

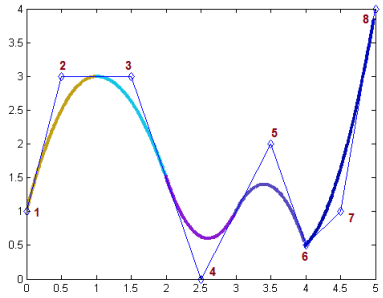

(d) B-spline curve with repeated knot

2.2.5 B-spline surfaces

Given two knot vectors $\xi = [\xi_1, \xi_2, \xi_3, ...\xi_{n+p+1}]$ and $\eta = [\eta_1, \eta_2, ...\eta_{m+q+1}]$ and control net $\boldsymbol{B}_{i,j}$, the B-spline surface is defined as

$$\mathcal{S}(\xi, \eta) = \sum_{i=1}^{n}\sum_{j=1}^{m} N_{i,p}(\xi)M_{j,q}(\eta)\mathcal{B}_{i,j} \tag{2.9}$$

$$\mathcal{S}(\xi, \eta) = \sum_{i=1}^{n}\sum_{j=1}^{m} N_{i,j}^{p,q}(\xi, \eta)\mathcal{B}_{i,j} \tag{2.10}$$

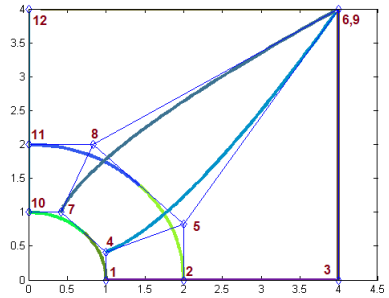

(e) Surface with Control Mesh

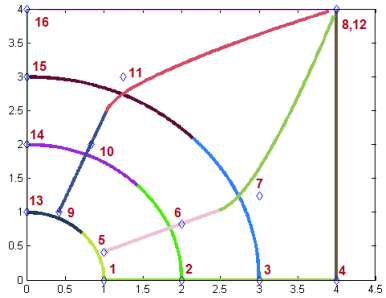

(f) Surface without Control Mesh

Figure 2.3: B-spline surfaces

2.3 NURBS

B-splines lack of ability to represent exactly the simple shapes such as circles and ellipsoids. So, Nurbs are used in CAD geomentries, which inherits all their favorable properties. They are useful to represent complex geometries.

2.3.1 NURBS basis functions

NURBS basis functions can be written as

$$\boldsymbol{R}_{i,p}(\xi) = \frac{\boldsymbol{N}_{i,p}(\xi)w_i}{\boldsymbol{W}(\xi)} = \frac{\boldsymbol{N}_{i,p}(\xi)w_i}{\sum_{j=1}^{n} \boldsymbol{N}_{j,p}(\xi)w_j} \tag{2.11}$$

2.3.2 NURBS curve

NURBS curve can be written as

$$\mathcal{C}(\xi) = \sum_{i=1}^{n} R_{i,p}(\xi)\mathcal{B}_i \tag{2.12}$$

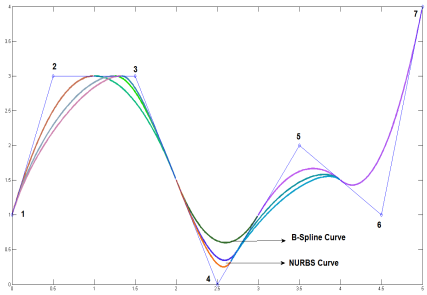

(a) NURBS Vs B-spline curve

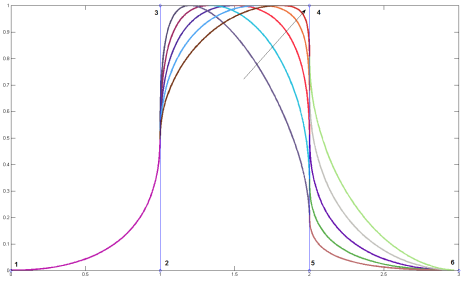

(b) Weight influence in NURBS

Figure 2.4: B-spline surfaces

2.3.3 NURBS surface

NURBS surface can be written as

$$\mathcal{S}(\xi,\eta) = \sum_{i=1}^{n}\sum_{j=1}^{m} R_{i,j}^{p,q}(\xi,\eta)\mathcal{B}_{i,j} \tag{2.13}$$

where,

$$R_{i,j}^{p,q}(\xi,\eta) = \frac{N_i(\xi)M_j(\eta)w_{i,j}}{\sum_{i=1}^{n}\sum_{j=1}^{m} N_i(\xi)M_j(\eta)w_{i,j}} \tag{2.14}$$

2.4 Finite element analysis with NURBS

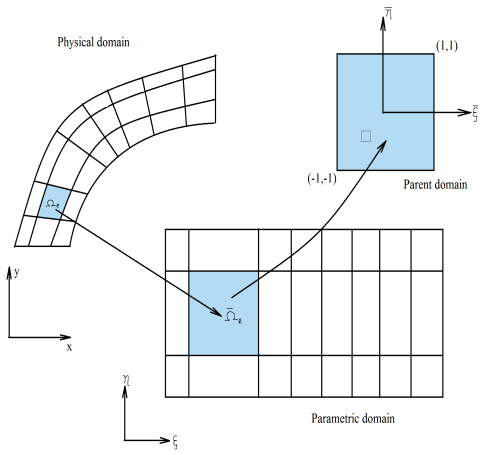

By following isoparametric discretisation, the mapping from parametric domain to the physical domain is given by

$$\mathrm{x} = \sum_{I=1}^{n} \Phi_I(\xi)\mathcal{B}_I \tag{2.15}$$

The displacement field is approximated by same basis functions as

$$\mathrm{u(x)} = \sum_{I=1}^{n} \Phi_I(\xi)\mathrm{u}_I \tag{2.16}$$

The Galerkin formulation of linear elasticity is employed. Gaussian quadrature is used on element for numerical integration.

2.5 Node moving adaptive refinement strategy in Isogeometric Analysis

2.6 Introduction

Finite element method has been successfully used for the simulation of a broad range of applications in last decades. The method, however, encounters some difficulties when dealing with problems involving moving boundaries, crack propagation or extremely large deformation due to their need for re-meshing of the domain. This problem, to a lesser degree, is also faced when exploiting the most important advantage of FEM over other mesh based numerical methods, namely adaptive refinement of the solution, where the mostly used method of h-refinement requires adding or repositioning of the nodal points. Different methodologies have been suggested by FEM researchers to overcome this problem with varying degrees of success. These methods, however, either partially solve the problem or are computationally very demanding. This has motivated the numerical activists to seek for a method that totally circumvents the mesh connectivity requirement of the FE and other mesh based methods. In the last decade, a wide range of methods referred to as meshless methods have

been devised in an attempt to overcome this problem. These methods are common in that they do not require a mesh with predefined connectivity among the nodes. Some important examples of these methods are the smoothed particle hydrodynamic (SPH) method, Reproducing Kernel Particle Method (RKPM), Element Free Galerkin (EFG) method, Meshless Local PetrovGalerkin (MLPG) method, Local Boundary Integral Equation (LBIE) method and hp-cloud method.

2.6.1 Isogeometric shape functions

Consider the following general partial differential equation governing a general elasticity problem

$$\boldsymbol{L(\Phi)} + \boldsymbol{f} = 0 \quad in\omega \tag{2.17}$$

subject to appropriate Dirchet and Neumann boundary conditions as

$$\Phi - \bar{\Phi} = 0 \quad on \quad \gamma_u \tag{2.18}$$

$$\boldsymbol{L}^1(\Phi) - \bar{t} = 0 \quad on \quad \gamma_t \tag{2.19}$$

where $\bar{\Phi}$ and $\bar{t}$ are vector of prescribed displacements and tractions on the Dirchlet and Neumann boundaries, respectively; γ_u and γ_t are the displacement and traction boundaries respectively; f is the vector of external force or source term on the problem domain; Φ is the vector of unknowns defined as $\Phi = [uv]^T$; $\boldsymbol{L}$ is a second order partial differential operator defined as

$$\boldsymbol{L}(.) = \boldsymbol{L_1}(.)_{xx} + \boldsymbol{L_2}(.)_{yy} + \boldsymbol{L_3}(.)_{xy} \tag{2.20}$$

where $\boldsymbol{L_1}$, $\boldsymbol{L_2}$, $\boldsymbol{L_3}$ are defined by the following matrices

$$\boldsymbol{L}_1 = \begin{bmatrix} \lambda + 2\mu & 0 \\ 0 & \mu \end{bmatrix}, \quad \boldsymbol{L}_2 = \begin{bmatrix} \mu & 0 \\ 0 & \lambda + 2\mu \end{bmatrix}, \quad \boldsymbol{L}_3 = \begin{bmatrix} 0 & \lambda + \mu \\ \lambda + \mu & 0 \end{bmatrix}$$

with λ, μ as the Lame constants defined as

$$\mu = \frac{\boldsymbol{E}}{2(1+\nu)}, \frac{\boldsymbol{E}\nu}{(1-2\nu)(1+\nu)} \tag{2.21}$$

in which ν is the poisson ratio and $\boldsymbol{E}$ is the young modulus. $\boldsymbol{L}^1$ is the first order differential operators representing the traction boundary condition as follow

$$\boldsymbol{L}^1(.) = \boldsymbol{L}^1_{\boldsymbol{1}}(.)_x + \boldsymbol{L}^1_{\boldsymbol{2}}(.)_y on \gamma_t \tag{2.22}$$

Assume that the problem domain is discretized using a set of nodal points arbitrarily distributed on the problem domain and its boundaries, then the residual of governing differential equation at a typical point k, which may or may not be a nodal point as

$$\boldsymbol{R}_\omega(x_k) = \boldsymbol{L}(\Phi(x_k)) + \boldsymbol{f}(x_k) \tag{2.23}$$

where N is the total number of nodes used to discretize the problem domain and its boundaries. Similarly, the residual of the Neumann boundary condition at a typical point k on the Neumann

boundary can also be written as

$$\boldsymbol{R}_t(x_k) = \boldsymbol{L}^1(\Phi(x_k)) - \boldsymbol{t}(\bar{x}_k) \tag{2.24}$$

And finally the residual of the Dirichlet boundary condition at a typical point on the Dirichlet boundary could be stated by

$$\boldsymbol{R}_u(x_k) = \Phi - \Phi(\bar{x}_k) \tag{2.25}$$

2.7 Error indicator

Adaptivity is an important tool for improving the efficiency of numerical methods. Any adaptive procedure is composed of two main components of error estimation and mesh refinement. For any successful adaptive procedure, a reliable error estimator is essential. For any successful adaptive procedure, a reliable error estimators have been devised and used with different numerical methods and in particular with the FEM. These methods can be divided into two broad classes namely residual based methods and recovery based methods. In the first method, the residual of the differential equation or some function of the residual is used as a measure of the error. The second approach uses the error in the gradient of the solution as a measure of the error. These errors are simply calculated by obtaining improved values of gradients using some of the available recovery processes. In this study, an error indicator used for the nodal refinement is simply defined as

$e_k = \sqrt{R(x_k)}$,

where, e_k is the value of error indicator at an arbitrary point on the problem domain or its boundaries.

2.8 Adaptive Refinement

Once the distribution of error is available via the error estimator, one can use any of the refinement techniques to adapt the numerical approximation such that an improved solution is obtained by resolution the problem. Generally speaking, there are three refinement approaches. The first one is H-refinement in which the grid spacing is adapted locally or globally in such a way to increase local and global accuracy by introducing more points on the areas of high errors. Once the distribution of error is available via the error estimator, one can use any of the refinement techniques to adapt the numerical approximation such that an improved solution is obtained by resolution the problem. Simultaneous application of h-and p-refinements leads to a third adaptive approach referred to as hp-refinement. H-refinement, which is the mostly used of the existing methods, can be carried out in three distinct ways. In the first method, referred to as mesh moving method, the number of nodes is kept fixed and they are relocated according to error distribution over the domain. This method has the advantage of computational efficiency since it does not lead an increase in the computational effort required to resolve the problem. The method, however, can face some difficulty when used with mesh based methods due to mesh distortion.

Mesh enrichment is an alternative method of h-refinement in which the original nodes are kept fixed and additional nodes are added in the areas suggested by the predicted error distribution. This

method may also face mesh distortion problem and many techniques have proposed to overcome the problem in the context of mesh based methods. This method is more effective than the mesh moving method but lacks efficiency due to an increase in the number of nodes required to represent the computational domain for desired accuracy. In the third method referred to as remeshing approach, a completely new mesh is created from the error calculated from the solution obtained on the previous mesh. The method requires an extra effort to transfer the solution from the old mesh over to the new mesh via interpolation. This method has been shown to be more effective and efficient compared to alternative methods while requiring complex meshing algorithm.

Many different mesh moving algorithms have been proposed and used for various problems. Amongst the existing algorithms, four methods namely trans-finite interpolation, isoparametric mapping, elastic analogy, and the spring analogy are mostly used. TFI and isoparametric mapping are algebraic algorithms, which are more suited to structured meshes in simple domains. The elastic analogy and spring analogy on the other hand, are applicable to both structured and unstructured meshes and therefore are more suitable to be used with meshless methods. Among the moving mesh algorithms, the spring analogy is more favored because of its simplicity, flexibility, and less memory requirements. A major drawback of mesh moving approach when used in conjunction with the mesh based methods such as FEM is that element inversion may happen. This, however, presents no problem when the method is used with meshless methods because they do not require any mesh connectivity. Spring analogy models can, in turn, be categorized into two types: vertex models and segment models. Vertex models springs are mainly used for mesh smoothing because the vertex springs are always under tension unless the spring length is zero.

When distribution of the error over the domain is defined by the proposed error indicator, refinement process must move the nodes to the areas, which have a larger quantity of error. Application of the spring analogy method requires that each nodal point is connected to some other nodes via springs of prescribed stiffness to form a spring system. Theoretically, there is no limit to the number of nodes that can be connected to an arbitrary point, but it is usual to connect each node to its neighboring nodal points. Upon calculating erros with appropriate boundary conditions, the refined postion of nodes is obtained leading to substantial reduction of the local and global eror of the numerical solution in the subsequent analysis. The efficiency and effectiveness of the proposed adaptive refinement technique is verified in the next section by its application to some benchmark test examples in elasticity.

2.9 Numerical Examples

2.9.1 Example-1

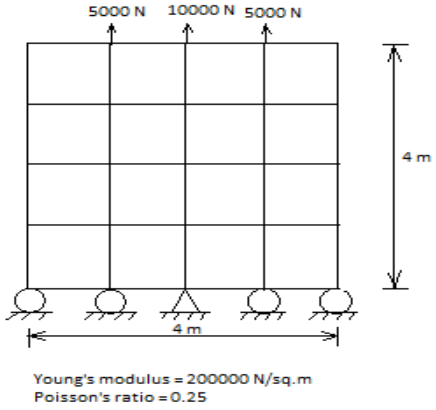

Figure 2.5: Block under Compression

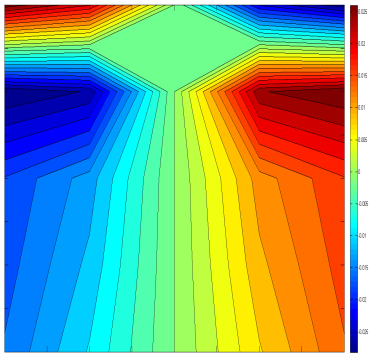

(a) Displacement in x-direction

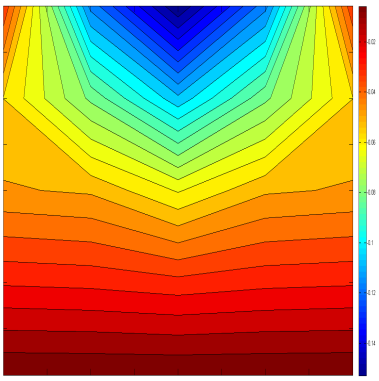

(b) Displacement in y-direction

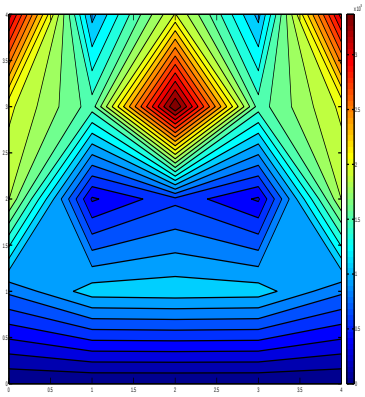

(c) Distribution of residual error

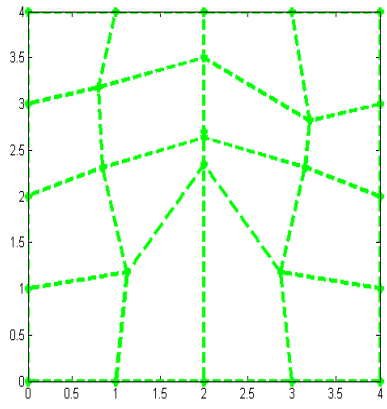

(d) Relocated final position of control points

2.9.2 Example-2

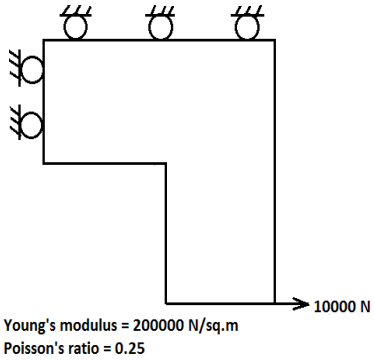

Figure 2.6: L-shaped domain

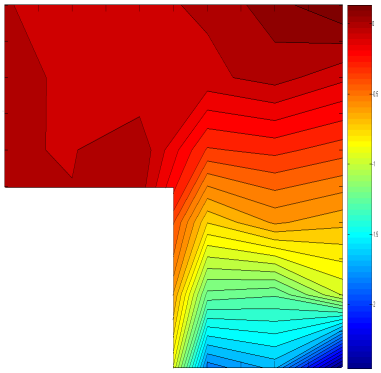

(a) Displacement in x-direction

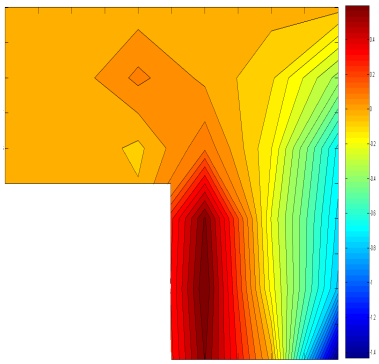

(b) Displacement in y-direction

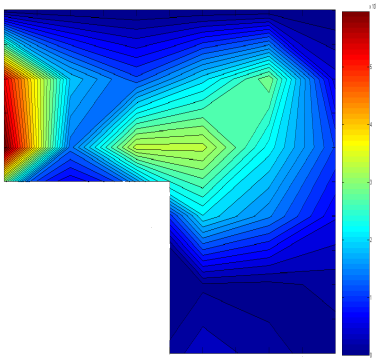

(c) Distribution of residual error

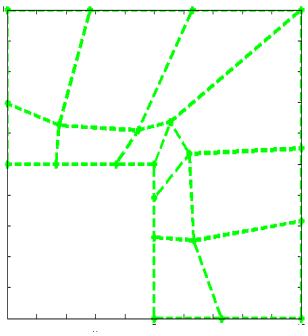

(d) Relocated final position of control points

Chapter 3

Higher gradient continuum theory of phenomenological isotropic plasticity

The framework, which was derived earlier is, at first, applied to the geometrically linear case of phenomenological elasto-plasticity in this chapter. The main focus will thereby be on theoretical and algorithmic aspects of a gradient formulation in terms of a case study. In addition to physical considerations, the following proposed gradient plasticity formulation is based on the observation that numerical computations of localized plastic deformations in softening materials, within a finite element setting, lead to results which depend in a pathological way on the chosen discretization. For example, shear bands in ductile materials are thereby resolved with a zero lateral width for the limiting case of infinitely refined discretizations. Clearly, in contrast to experimental observations, this unphysical behavior motivates so-called regularization methods to overcome these numerical difficulties. For the present case of phenomenological gradient plasticity, the regularizing behavior is emphasized with a loss of ellipticity analysis since loss of ellipticity corresponds to the onset of localization.

In particular, computational gradient models at the macro-level were proposed by the Dutch school, e.g., [12], [13],[14], [15]. One can thereby differentiate explicit gradient models on the one hand and implicit models on the other hand, see [16] and [17] in case of fracture mechanics or [18], [19] in case of softening plasticity for a discussion of these models. Thermodynamically motivated formulations of gradient plasticity were derived by [] in the spirit of the theory, which is being focused on in this thesis. The goal of this chapter is therefore to set up the theory and the numerics of a thermodynamically consistent formulation of gradient plasticity at small strains. Starting from the classical local continuum formulation, which fails to produce physically meaningful and numerically converging results within localization computations, a thermodynamically motivated gradient plasticity formulation is envisioned.

The model is based on an assumption for the Helmholtz free energy incorporating the gradient of the internal history variable. For compatibility requirements between the internal variable and its gradient, (i) a nonlocality residual in the local dissipation inequality is incorporated, (ii) a bilinear

form for the dissipation density is introduced and (iii) the insulation condition is applied to render the quasi-nonlocal drag stress, which is conjugated to the independent history variable .

Then, based on a phenomenological yield condition and the postulate of maximum dissipation, an associated structure is achieved. As the distinctive feature, the Karush-Kuhn-Tucker conditions depend on the quasi-nonlocal drag stress. Furthermore, constitutive and continuity boundary conditions are derived. On the numerical side, due to this special structure, an active set search becomes necessary for the monolithic iterative solution of the phenomenological isotropic gradient plasticity coupled problem within a typical Newton-Raphson strategy. In particular, it is notable that the additional discrete algorithmic loading and unloading conditions complemented by an active set search are implemented on a nodal basis. The simultaneous solution of the discrete algorithmic Karush-Kuhn-Tucker conditions in addition to the discretized algorithmic balance of linear momentum offers an elegant solution strategy in the numerical treatment of gradient plasticity. The extension to the geometrically nonlinear case follows in the example section.

3.1 Strain gradient plasticity theories

The homogeneous flow stress can we written as

$$\sigma_f = \sigma_{ref} + Hf(p) \tag{3.1}$$

The above equation cannot predict inhomogeneous deformations. So, it should be modified as

$$\sigma_f = \sigma_{ref} + H[f(p)^{\gamma_1} + g(l^n \eta_n)^{\gamma_2}]^{\frac{1}{m*\gamma_3}} \tag{3.2}$$

where,

$$g = l|| \bigtriangledown p|| + l^2 \bigtriangledown^2 p \tag{3.3}$$

Here, the first gradients takes presence of GND's into account and describe size effects at micron or submicron level. The second gradients gives objective results for localization problems.

3.2 Thermodynamics of phenomenological local plasticity

In classical local plasticity the free Helmholtz energy ψ is a function of the elastic macroscopic strain and a microscopic history variable κ which characterizes isotropic hardening effects. So, Helmholtz free energy function can be written as

$$\psi(\epsilon, \epsilon^p, \kappa) = \psi^{mac}(\epsilon - \epsilon^p) + \psi^{har}(\kappa) \tag{3.4}$$

Then, exploiting the Clausius-Duhem inequality for the local dissipation given as

$$\boldsymbol{D} = \sigma : \dot{\epsilon} - \dot{\psi} \tag{3.5}$$

renders the constitutive relations for the macroscopic stress σ, the dissipative stress σ^p and the drag stress $H = H(\kappa)$ as thermodynamically conjugated to ϵ^p and κ. Macroscopic stress can be

defined as

$$\sigma = \frac{\partial \psi^{mac}}{\partial \epsilon} \tag{3.6a}$$

Dissipative stress can be defined as (3.6b)

$$\sigma^p = \frac{\partial \psi^{mac}}{\partial \epsilon^p} = -\sigma \tag{3.6c}$$

Drag stress can be defined as (3.6d)

$$H = \frac{\partial \psi^{har}}{\partial \kappa} \tag{3.6e}$$

The Dissipation inequality is written as

$$D = -\sigma^p : \dot{\epsilon^p} - H\dot{\kappa} \geq 0 \tag{3.7}$$

A yield function incorporating isotropic hardening is readily motivated as

$$\Phi(\sigma, H) = \varphi(\sigma) - Y = \varphi(\sigma) - [Y_0 + H] \leq 0 \tag{3.8}$$

whereby, the equivalent stress $\varphi(\sigma)$ is introduced, preferably homogeneous of degree one in σ, together with the initial yield stress Y_0 and the current yield stress $Y = Y_0 + H$.

Then, based on postulate of maximum dissipation, the constrained optimization problem is given as

$$\mathcal{L}\left(\sigma, H, \dot{\epsilon^p}, \dot{\kappa}, \lambda\right) = -\mathcal{D} + \lambda\Phi = -\sigma : \dot{\epsilon^p} + H\dot{\kappa} + \lambda\Phi\left(\sigma, H\right) \tag{3.9}$$

Based on postulate of maximum dissipation, the evolution laws can be written as

$$\dot{\epsilon^p} = \lambda\frac{\partial \Phi}{\partial \sigma} = \lambda\frac{\partial \varphi}{\partial \sigma} \tag{3.10a}$$

$$\dot{\kappa} = -\lambda\frac{\partial \Phi}{\partial H} = \lambda \tag{3.10b}$$

Kuhn-Tucker conditions and consistency conditions are

$$\Phi\left(\sigma, H\right) \leq 0 \tag{3.11a}$$

$$\lambda \geq 0 \tag{3.11b}$$

$$\lambda\Phi\left(\sigma, H\right) = 0 \tag{3.11c}$$

$$\lambda\dot{\Phi}\left(\sigma, H\right) = 0 \tag{3.11d}$$

3.3 Thermodynamics of Phenomenological Gradient Plasticity

Helmholtz free energy is a function of macroscopic strain and a scalar valued internal history variable κ representing isotropic hardening mechanisms together with its first gradient $\bigtriangledown\kappa = \boldsymbol{\kappa}$ characterizing micro-structural interactions related to geometrically necessary dislocations.

Helmholtz free energy function for geometrically linear case is given as

$$\psi = \psi\left(\epsilon, \epsilon^p, \kappa, \boldsymbol{\kappa}\right) = \psi^{mac}\left(\epsilon - \epsilon^p\right) + \psi^{har}\left(\kappa\right) + \psi^{dis}\left(\boldsymbol{\kappa}\right) \tag{3.12}$$

Hardening flux which is thermodynamically conjugated to $\boldsymbol{\kappa}$ is given as

$$\boldsymbol{H} = \frac{\partial \psi^{grd}}{\partial \boldsymbol{\kappa}} \tag{3.13}$$

Consequently, the dissipation inequality now is

$$\mathcal{D} = -\sigma^p : \dot{\epsilon^p} - H\dot{\kappa} - \boldsymbol{H} \cdot \dot{\boldsymbol{\kappa}} + \mathcal{P} = \sigma : \dot{\epsilon^p} - H\dot{\kappa} - \boldsymbol{H} \cdot \dot{\boldsymbol{\kappa}} + \mathcal{P} \tag{3.14}$$

Now that the present format of the dissipation inequality suggests two independent evolution laws for κ and $\boldsymbol{\kappa}$, but due to compatability between $\dot{\kappa}$ and $\dot{\boldsymbol{\kappa}} = grad\dot{\kappa}$, the evolution equations should be designed in such a way that compatability is satisfied.

$$\mathcal{D} = \sigma : \dot{\epsilon^p} - \bar{H}\dot{\kappa} \tag{3.15}$$

So, by comparing both dissipation inequalities, the nonlocality residual is

$$\mathcal{P} = H\dot{\kappa} + \boldsymbol{H} \cdot \dot{\boldsymbol{\kappa}} - \bar{H}\dot{\kappa} \tag{3.16}$$

Again applying the insulation condition, integration by parts and invoking Gauss theorem renders

$$\int_{\mathcal{B}^p} \mathcal{P}\, dV = \int_{\mathcal{B}^p} \left[H - \mathrm{div}\boldsymbol{H} - \bar{H}\right] \dot{\kappa}\, dV = \int_{\partial\mathcal{B}^p} \left[\boldsymbol{n} \cdot \boldsymbol{H}\right] \dot{\kappa}\, dA = 0 \tag{3.17}$$

So, from insulation condition we have

$$\bar{H} = H - \mathrm{div}\boldsymbol{H} \quad \text{in} \quad \mathcal{B}^p \quad \text{and} \quad \left[\boldsymbol{n} \cdot \boldsymbol{H}\right] \dot{\kappa} = 0 \quad \text{on} \quad \partial\mathcal{B}^p \tag{3.18}$$

Consequently, for the present case of gradient plasticity, based on the local dissipation inequality ≤ 0 in bilinear form, a yield condition is readily motivated as

$$\Phi\left(\sigma, \bar{H}\right) = \varphi\left(\sigma\right) - \left[Y_0 + \bar{H}\right] \leq 0 \tag{3.19}$$

Note that the quasi-nonlocal current yield stress $\bar{Y} - Y_0 + \bar{H}$. The postulate of maximum dissipation is

$$\mathcal{L}\left(\sigma, \bar{H}; \dot{\epsilon^p}, \dot{\kappa}, \lambda\right) = -\mathcal{D} + \lambda\Phi = -\sigma : \dot{\epsilon^p} + \bar{H}\dot{\kappa} + \lambda\Phi\left(\sigma, \bar{H}\right) \tag{3.20}$$

Remarkably, the evolution equations retain the same format as for the gradient and local plas-

ticity.

3.4 Numerical treatment of phenomenological gradient plasticity

For gradient continua, a variety of numerical strategies by [20], [18], [21], [22], [23], [24], [1]. Furthermore, [25] studied the influence of the discretization on the regularization performance of different localization limiters. Further contributions to the numerics of phenomenological gradient plasticity at small and large strains were treated by [26]. Alternatively, [25] recently proposed an implicit BEM-formulation for gradient continua and localization phenomena. For the local continuum description an early attempt to set up a mixed finite element formulation was provided by [27], whereby a plastic strain-like variable is discretized in addition to the displacement field. An alternative proposal based on a complementary mixed finite element formulation is due to [28], wherein the flow rule is enforced in a weak sense at the element level. Likewise, a two-field finite element formulation for elasticity coupled to damage was proposed by [22].

3.5 Strong form of coupled problem

Let $\boldsymbol{B}$ denote the configuration occupied by an elasto plastic solid. Then, displacement field $u = u(x)$ and history variable field κ=κ(x) are in terms of displacement at x. These fields are determinded by the simultaneous solution of partial differential equation and a set of Kuhn-Tucker conditions. Firstly, neglecting inertia, the equilibrium subproblem $r^u(u, \kappa)$ is given by the quasi-static balance of linear momentum in $\boldsymbol{B}$ as given below, whereby distributed body forces per unit volume in $\boldsymbol{B}$ are denoted by b. Thereby, for the displacement field the decomposition of the total boundary leads to

$$\partial \boldsymbol{B} = \partial \boldsymbol{B}^u \cup \partial \boldsymbol{B}^t with \partial \boldsymbol{B}^u \cap \partial \boldsymbol{B}^t = \phi \tag{3.21}$$

Equilibrium subproblem is

$$r^u(\boldsymbol{u}, \kappa) = \mathrm{div}\sigma(\boldsymbol{u}, \kappa) + \boldsymbol{b} = 0 \quad \text{in} \quad \mathcal{B} \tag{3.22a}$$

$$\boldsymbol{u} - \boldsymbol{u}^p = 0 \quad \text{on} \quad \partial\mathcal{B}^u \tag{3.22b}$$

$$\boldsymbol{n} \cdot \boldsymbol{\sigma}(\boldsymbol{u}, \kappa) - \boldsymbol{t}^p = 0 \quad \text{on} \quad \partial\mathcal{B}^t \tag{3.22c}$$

Constitutive subproblem is

$$r^\Phi(\boldsymbol{u}, \kappa) = \varphi(\boldsymbol{u}, \kappa) - \bar{Y}(\kappa) \leq 0 \quad \text{in} \quad \mathcal{B} \tag{3.23a}$$

$$\dot{\kappa} = 0 \quad \text{on} \quad \partial\mathcal{B}^p_{int} \tag{3.23b}$$

$$\boldsymbol{n} \cdot \boldsymbol{H}(\kappa) = 0 \quad \text{on} \quad \partial\mathcal{B}^p_{ext} \tag{3.23c}$$

The balance of linear momentum is thus supplemented by Dirichlet and Neumann boundary conditions in terms of the displacement u on $\partial \boldsymbol{B}^u$ and the traction vector t on $\partial \boldsymbol{B}^t$, respectively.

Secondly, the constitutive subproblem is incorporated by the yield condition $r^{\Phi}(\boldsymbol{u}, \kappa)$, which incorporates the quasi-nonlocal yield stress $\bar{Y} = Y_0 + \bar{H}$ in terms of the quasi nonlocal brag stress $\bar{H} = H - div\boldsymbol{H}$ together with the corresponding Karush-KUnh-Tucker complementary conditions.

3.6 Spatial Discretization of the coupled problem

Finally, the algorithmic set of equations has to be discretized in space. To this end, the standard Bubnov-Galerkin finite element method is employed. The whole solution domain $\boldsymbol{B}$ is decomposed into finite elements $\boldsymbol{B}_e$. Each element is characterized by nodal degrees of freedom due to the displacement field and additionally by nodal degrees of freedom due to the internal history variable field.

$$x^h|_{B_e} = \sum_k N_x^k x_k \qquad u^h|_{B_e} = \sum_k N_x^k u_k \tag{3.24a}$$

$$\delta u^h|_{B_e} = \sum_k N_x^k \delta u_k \qquad \kappa^h|_{B_e} = \sum_k N_x^k \kappa_k \tag{3.24b}$$

$$\delta \kappa^h|_{B_e} = \sum_k N_x^k \delta \kappa_k \qquad \delta\Phi|_{B_e} = \sum_k N_x^k \delta\Phi_k \tag{3.24c}$$

Equilibrium subproblem is

$$R_K^u\left(\boldsymbol{u}_{n+1}^h, \kappa_{n+1}^h\right) = \boldsymbol{A}_e \int_{\partial\mathcal{B}_e \cap \partial\mathcal{B}^t} N_x^k \boldsymbol{t}_{n+1}^p \, dA + \int_{\mathcal{B}_e} \left[N_x^k \boldsymbol{b}_{n+1} - \mathrm{grad} N_x^k \cdot \boldsymbol{\sigma}\left(\boldsymbol{u}_{n+1}^h, \kappa_{n+1}^h\right)\right] \, dV \tag{3.25a}$$

$$= 0 \quad \forall K \quad \text{in} \quad \mathbb{B}$$

Constitutive subproblem is

$$R_K^{\Phi}\left(\boldsymbol{u}_{n+1}^h, \kappa_{n+1}^h\right) = \boldsymbol{A}_e \int_{\mathcal{B}_e} \left[N_\kappa^k \left[\varphi\left(\boldsymbol{u}_{n+1}^h, \kappa_{n+1}^h\right) - Y\left(\kappa_{n+1}\right)\right] - \mathrm{grad} N_\kappa^k \cdot \boldsymbol{H}\left(\kappa_{n+1}^h\right)\right] \, dV \tag{3.26a}$$

$$\leq 0 \quad \forall K \quad \text{in} \quad \mathbb{B}$$

$$\triangle R_K^{\kappa}\left(\kappa_{n+1}^h\right) = \boldsymbol{A}_e \int_{\mathcal{B}_e} \left[N_\kappa^k \left[\kappa_{n+1}^h - \kappa_n^h\right]\right] \, dV \tag{3.26b}$$

$$\geq 0 \quad \forall K \quad \text{in} \quad \mathbb{B}$$

3.7 Numerical Examples

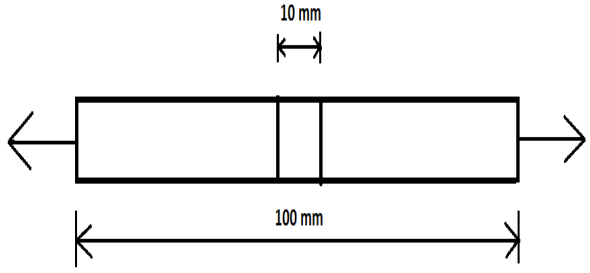

Figure 3.1: Bar example

With the above algorithm at hand, the performance of the proposed gradient formulation is now investigated. Firstly, a 1D-model problem of a bar loaded in uniaxial tension as frequently treated in the literature is analyzed

For the sake of demonstration, the bar loaded in uniaxial tension serves as a 1D-model problem that will be examined in the sequel. The problem statement, which includes a slight graded material imperfection in the middle of the bar. Whereby the previously derived constitutive and continuity boundary conditions were prescribed at the corresponding boundary. The material is modeled based on a one-dimensional von Mises yield function with isotropic linear hardening or softening.

Elastic Modulus $E = 1N/mm^2$, Initial yield strength $Y_0 = 0.01N/mm^2$, Reduced initial yield strength $Y0_r = 0.009N/mm^2$, Linear hardening modulus $H_0 = 1.5N/mm^2$, Linear softening modulus $H_0 = -.5N/mm^2$. The hardening and softening behaviour was modelled using different hardening and softening modulus.

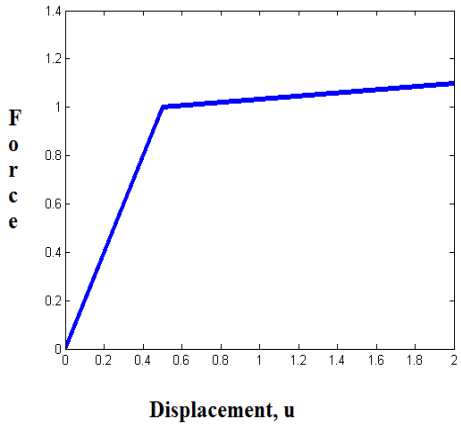

(a) Hardening behavior

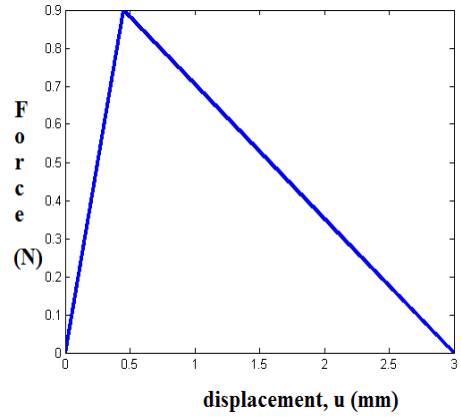

(b) softening behavior

Bibliography

[1] c. Chambon. One dimensional localisation studied with a second grade model 17, (1998) 637–656.

[2] T. V. Benallal, A. An implicit bem formulation for gradient plascity and localization phenomena. *Int.J.Num.Meth.Eng.* 53, (2002) 1853–1870.

[3] M. Jirasek and S. Rolshoven. A strain gradient theory of plasticity. *International Journal of Solids and Structures* 6, (1970) 1513–1533.

[4] G. Maugin. The method of virtual power in continuum mechanics; application to coupled fields. *Int.J.Solids struct* 35, (1980) 1–70.

[5] E. Aifantis. ON the microstructural origin of certain inelastic models 106, (1984) 326–330.

[6] A Phenomenological theory for strain gradient effects in plasticity .

[7] G. Maugin. The method of virtual power in continuum mechanics; application to coupled fields. *Int.J.Solids struct* 35, (1980) 1–70.

[8] Localization limiters in transient problems for strain softening in statics and dynamics .

[9] A. E. Muhlhaus, H. A variational principle for gradient plasticity. *Int.J.Solids struct* 28, (1991) 845–857.

[10] R. De borst. The thickness of shear bands in granular materials 37, (1987) 271–283.

[11] On the gradient dependent theory of plasticity and shear banding .

[12] R. Borst. Continuum models for discontinuous media. In:Fracture processes in Concrete, Rock and Ceramics. *Int.J.Solids struct* 34.

[13] S. L. Wave propagation, localization and dispersion in softening solids. Ph.d.dissertation. *Int.J.Solids struct* .

[14] P. J. Gradient-dependent plasticity in numerical simulation of localization phenomena .

[15] M. Geers. Experimental analysis and computational modellingof damage and fracture. Ph.D.thesis .

[16] R. Peerlings. Some observations on localization in non local and gradient damage models. *Int.J.Solids struct* 15, (1996a) 937–953.

[17] Localisation issues in local and nonlocal continuum approcaches to fracture .

[18] P. J. Gradient-dependent plasticity in numerical simulation of localization phenomena, Ph.d.dissertation, Delft University of Technology, Delft .

[19] Comparison of integral type nonlocal plasticity models for strain gradient softening materials .

[20] sluys L. Wave propagation, localization and dispersion in softening solids. Ph.d.dissertation, Delft university of Technology, Delft .

[21] P. J. de Borst, R. Some novel developments in finite element procedures for gradient-dependent plasticity and finite elements. *International Journal of Numerical Methods in Engineering* 39, (1996) 2477–2505.

[22] d. B. R. peelings, R. Gradient enhanced damage for quasi brittle materials. *International Journal of Numerical Methods in Engineering* 39, (1996b) 3391–3403.

[23] P. Steinmann. Formulation and computation of geometrically non-ninear gradient damage. *International Journal of Numerical Methods in Engineering* 37, (1999) 7371–7391.

[24] C. Comi. Computational modelling of gradient enhanced damage in quasi brittle materials 4, (1999) 17–36.

[25] T. V. Benallal, A. An implicit bem formulation for gradient plascity and localization phenomena. *Int.J.Num.Meth.Eng.* 53, (2002) 1853–1870.

[26] T. svedberg. On the modeling and numerics of gradient regularized plasticity coupled to damage. Ph.D.thesis 161, (1999) 49–65.

[27] p. Pinsky. A finite element formulation for elasto plasticity based on a three field variations equation. *Compu. Methods Appl.Mech.Emgrg* 61, (1986) 41–60.

[28] K. J. T. R. Simo, J. Complementary mixed finite element formulations for elasto plasticity 74, (1989) 177–206.